FULL PAPER

Self-Assembly Mechanism of Spiky Magnetoplasmonic Supraparticles

Hongjian Zhou, Jong-Pil Kim, Joong Hwan Bahng, Nicholas A. Kotov,* and Jaebeom Lee*

Concave nanoparticles (NPs) with complex angled and non-Platonic geometries have unique optical, magnetic, catalytic, and biological properties originating from the singularities of the electrical field in apexes and craters. Preparation of such particles with a uniform size/shape and core–shell morphology represents a significant challenge, largely because of the poor knowledge of their formation mechanism. Here, this challenge is addressed and a study of the mechanism of their formation is presented for a case of complex spiky morphologies that led us to the conclusion that NPs with concave geometries can be, in fact, supraparticles (SPs) produced via the self-assembly of smaller convex integrants. This mechanism is exemplified by the vivid case of spiky SPs formed via the attachment of small and faceted Au NPs on smooth Au-coated iron oxide (Fe$_3$O$_4$@Au) seeds. The theoretical calculations of energies of primary interactions—electrostatic repulsion and van-der Waals repulsion, elaborated for this complex case—confirm experimental observation and the self-limiting mechanism of SP formation. Besides demonstrating the mechanistic aspects of synthesis of NPs with complex geometries, this work also uncovers a facile approach for preparation of concave magnetoplasmonic particles. When combined with a spiky geometry, such bi-functional magnetoplasmonic SPs can serve as a unique platform for optoelectronic devices and biomedical applications.

1. Introduction

Synthesis of noble-metal nanoparticles (NPs) with highly controlled non-spherical shapes represents challenging and rapidly developing area of nanochemistry. A particularly interesting topic in this field is the synthesis and properties of NPs with concave nanoscale geometries. These NPs have distinct "spiky" shapes, with apexes that give rise to multiple optical, chemical, biological effects. NPs typically have Platonic geometries, which include tetrahedrons, cubes, hexahedrons, octahedrons, dodecahedrons, and icosahedrons, representing five regular tessellations of the sphere. Some examples of Archimedean and Johnson solids can also be found among NPs.[1–3] From a geometrical perspective, all shapes mentioned above are convex. Concave NPs are much less common and, while known,[4–9] their formation mechanism is still enigmatic. A large surface area, plasmonic hot spots, strong near-infrared absorbance, and special interactions with cells and cell components[10–27] differentiate concave spiky particles from NPs with spherical and/or other convex shapes. All of these properties have high practical relevance and, apart from the fundamental interest, make it possible to substantially advance NP applications in catalysis, photonics, electronics, plasmonics, sensing, biological labeling, imaging, and cancer therapy.

In general, the spiky particles are thermodynamically unstable and can potentially transform into spherical particles with time.[28] The synthesis conditions for them were identified serendipitously, which does negate their importance or uniqueness but rather underlines the need to understand the underlying reasons for such growth pattern seeming deviating from thermodynamic control elaborated for "smooth" particles with Platonic shapes. While many papers do not describe the mechanism of formation of the spikes and focus primarily on the unusual morphology and optical properties of corresponding dispersions,[17,29,30] the formation of the spiked or bristled particles is currently attributed to different tendency of the stabilizers exemplified by thioglycolic acid,[31] poly(vinylpyrrolidone) (PVP),[6] or cetyltrimethylammonium bromide (CTAB),[7] to absorb on diverse crystal faces.[6,8] The pivotal role of surface defects on NP seeds increasing in numbers under rapid growth conditions was also suggested as potential reason for the growth of spikes.[7]

These explanations involving the thermodynamically controlled variability of stabilizer density and kinetically controlled density of defects as well as the combination thereof, however,

H. Zhou
Department of Nano Fusion Technology
Pusan National University
627–706, Republic of Korea
Dr. J.-P. Kim
High Technology Components &
Materials Research Center
Korean Basic Science Institute
Busan, 609–735, Republic of Korea
J. H. Bahng, Prof. N. A. Kotov
Department of Chemical Engineering
Materials Science, and Biomedical Engineering
University of Michigan, Ann Arbor
Michigan, 48109, USA
E-mail: kotov@umich.edu
Pro. J. Lee
Department of Nano-Integrated Cogno-mechatronics
Engineering (NICE)
Pusan National University
Busan, 609–735, Republic of Korea
E-mail: jaebeom@pusan.ac.kr

DOI: 10.1002/adfm.201302405

are difficult to accept because the spikes grow without an apparent symmetrical relation between them. Also, the growth of the spikes occurs on seeds coated with different surfactants and displaying a variety of atomic faces including smooth surfaces of fairly large rods and beads.[32] The view of surface defects as the primary factor in production of spiky particles is difficult to rationalize in the view of the high crystallinity of the resulting particles.

Some of these controversies originate from the atom-by-atom model for the growth of nanoparticle that start with seeds of critical size and grow according to the kinetics of ion/atom attachment to different crystal faces.[35,36] However, this model does not always determine the growth of the particles and, in particularly their shapes.[27,37,38] One should also notice that rapid growth conditions are common requirement for a variety of nanocolloids where the growth of spiky NPs were demonstrated.[33,34] Both of these observations led us to consider an alternative mechanism for the formation of spiky particles and other complex non-Platonic shapes. Recently, the concept of a self-limiting process was suggested as a way of growing monodispersed supraparticles (SPs), mimicking the supramolecular assemblies that occur in proteins, such as in viral capsids.[39] The size of SPs is quite similar to the dimensions of spiky particles made so far and their surface also display similar roughness.[39] The yield of SPs approached 100% is also similar to the yields observed for some spiky particles.[6] Such similarities are unlikely (although possible) to be coincidental and in this work we decided to investigate the growth of spiky NPs having from the perspective of potential SP involvement in their formation. We demonstrate here successful synthesis of spiky core-shell particles that are, in fact, self-assembled SPs made from Au and Fe_3O_4 NPs (**Scheme 1**). We also present experimental and theoretical data supporting the idea that spiky shapes are produced not due local kinetic or structural in homogeneities but due to self-assembly of individual NPs generated in-situ into larger structures. We believe that these findings will help to understanding the mechanism(s) governing the formation of spiky particles better and can open the door to synthesis of even more complex concave non-Platonic shapes. As such, the careful evaluation of the mechanistic aspects of "spiky" synthesis, SPs made from Au and Fe_3O_4 NPs represent the first example of nanoscale convex particles combining two inorganic

nanomaterials: magnetic and plasmonic. Consideration of SP self-assembly route makes possible to form SPs[30] with spiky shape, tunable diameters (ca. 95–185 nm), plasmonic absorption in 600–700 nm region and strong magnetization.

2. Results and Discussion

2.1. Synthesis and Structure

We decided to approach the problem of their synthesis from the perspective of the assembly of NPs on pre-made nanoscale cores considering that the attachment of the additional nanoscale "building blocks" will be controlled by the balance of attractive and repulsive interactions as was demonstrated in a previous publication.[39] This approach is consistent with the previously reported protocols for synthesis of spiky particle under different conditions.[7,30–32] One substantial difference is that the resulting SPs could correspond to the state of local thermodynamic minimum, which makes it possible to accurately control their diameter. Alternatively, the availability of the total amount of the additional constituent NPs can also control their size. The self-assembly approach allows one to mix-and-match different types of NPs starting with one type and making a shell around it from another type, which is an additional advantage that let to our interest in this process.

We started with citrate-stabilized Fe_3O_4 NPs made by conventional approach. A transmission electron microscopic (TEM) images of the resulting NPs is shown in **Figure 1**a. These initial Fe_3O_4 NPs were almost spherical with average size ~10 nm, as seen in the high magnification TEM micrograph in Figure S1 and the particle size distribution in Figure S2–A. After fabricating the magnetic cores, we coated them with the first layer of Au to produce spherical Fe_3O_4@Au core–shell particles with a smooth surface (Figure 1b). These particles served as seeds for assembling the SPs. The synthesis of smooth, spherical Fe_3O_4@Au core–shell particles was accomplished by adding Fe_3O_4 NPs to boiling $HAuCl_4$ in the presence of citrate as a stabilizer and a reducing agent (see Experimental Section).[58] The resulting fairly monodispersed Fe_3O_4@Au core–shell particles had purple color associated with the optical properties of the smooth shells of Au (Figure 1b) (average size is 25 ± 2.4 nm, Figure S2–B).[59]
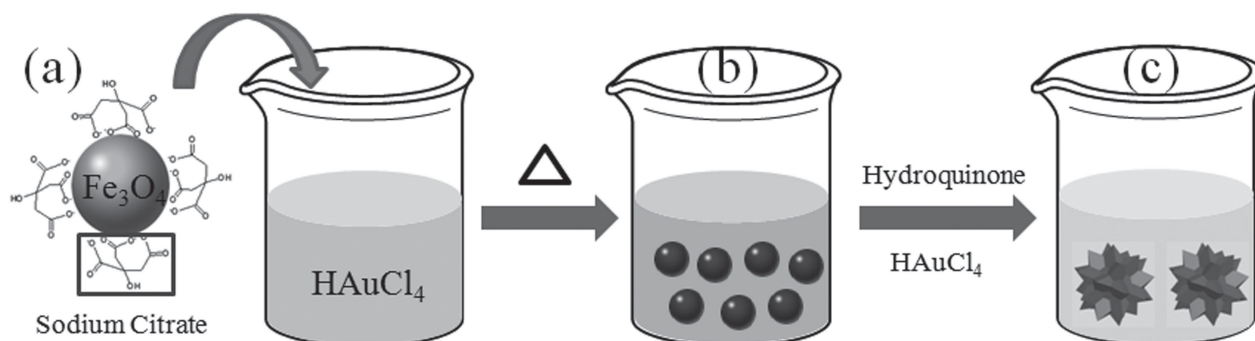
Scheme 1. Schematic for preparation of spiky Au-coated magnetic SPs: a) synthesis of spherical Fe_3O_4 NPs; b) deposition of a Au Fe_3O_4 NP layer to produce spherical Fe_3O_4@Au NPs; and c) assembly of in situ-generated active Au NPs on spherical Fe_3O_4@Au NPs to produce spiky SPs. (NP sizes are not to scale.)

www.MaterialsViews.com

ADVANCED
FUNCTIONAL
MATERIALS
www.afm-journal.de

FULL PAPER
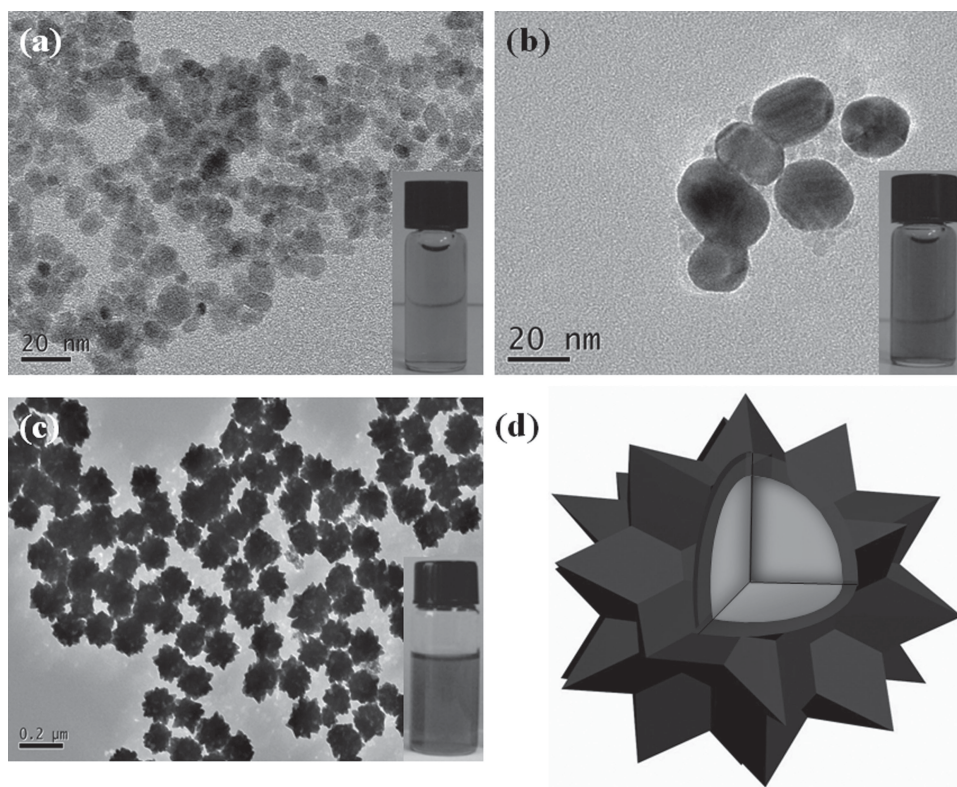
Figure 1. TEM images of a) Fe$_3$O$_4$ nanoparticles; b) nearly spherical Fe$_3$O$_4$@Au core–shell particles with smooth layer of gold; c) spiky SPs made by self-assembly of in situ-generated Au NPs on Fe$_3$O$_4$@Au core–shell particles; and d) a 3D schematic drawing of spiky SPs. Insets in each TEM image show the photograph of corresponding aqueous dispersions.

Small Fe$_3$O$_4$ NPs (~5 nm) not coated by Au shells were sometimes attached on the surface of larger Fe$_3$O$_4$@Au particles. The thickness of the Au shell is estimated to be around 7.5 ± 1.2 nm according to the TEM images in Figure 1a,b.

Combining scanning transmission electron microscopy (STEM) with energy-dispersive X-ray spectroscopy (EDXS) and scanning the NPs with 1.0-nm diameter beam, it was possible to distinguish the component elements, including Au, Fe and O (Figure S3). In the micrographs, Fe$_3$O$_4$ NPs coated with Au appear much darker than the uncoated Fe$_3$O$_4$ NPs because Au is more electron-dense than iron oxide. The line mapping of the selected NPs indicates the inclusion of a Fe core and a Au shell as a single Fe$_3$O$_4$@Au nanostructure.[60,61] The relative ratio of Au to Fe in the selected NP was found to be 16:1 (Figure S3–B). The EDXS maps show that Fe, Au and O are present in the same NPs, which is consistent with the core–shell morphology.

Instead of citrate, hydroquinone was used as reducing agent because the redox potential of hydroquinone, –0.699 V versus a normal hydrogen electrode (NHE), $Hydroquinone \Leftrightarrow 2H^+ + 2e + Benzoquinone,$[58,62] is substantially more negative than the redox potential of citrate, –0.5 V versus NHE, $Citric\ acid \Leftrightarrow CO_2 + H_2O + 2e + Acetonedicarboxylic\ acid$ [63,64] This difference in reduction potential resulted in the fast formation[65] of Au NPs when using hydroquinone. Although we expected these Au NPs to agglomerate with the premade smooth, spherical Fe$_3$O$_4$@Au core–shell particles serving

as seeds, these weakly stabilized NPs are expected to promote attractive interactions owing to low zeta potential value ($\zeta = -9.77$ mV) reported previously.[66]

The TEM images (Figure 1) show that the spiky morphology indeed gradually developed. The number of branches in the spiky SP$_S$ was approximately 25–30 per particle. The diameter of the spiky SPs was ca. 185 nm, resulting in distinct green dispersions (Figure 1c). The size distribution curve of the spiky SPs shows an average diameter of approximately 190 nm (Figure S2–C, Supporting Information). There were no significant absorption features in the visible region of the electromagnetic spectrum for dispersions of the starting Fe$_3$O$_4$ NPs. The surface plasmon peaks for the spiky Fe$_3$O$_4$@Au core–shell SPs appeared in the range 470–800 nm and differed markedly from the citrate-stabilized Au NPs in water, which exhibited a surface plasmon peak at 520 nm.[70] The AFM and SEM images of the smooth, spherical Fe$_3$O$_4$@Au seed NPs and spiky SPs is shown in Figure S4. Comparing Figure S4, we can clearly see the difference in the morphology between these two core–shell NPs. The spiky SPs show a rougher surface than the spherical NPs because of the presence of tips.

2.2. Mechanism of Formation

To support the hypothesis that the spiky particles observed in this synthetic process are, in fact, SPs formed as a result of

self-assembly and Fe_3O_4@Au core–shell particles are required to initiate the process, we evaluated the interaction potential at 3 chronological stages of assembly; interaction between hydroquinone reduced Au NPs and Fe_3O_4@Au core–shell (initial stage, stage i), intermediate SPs (growth stage, stage g) and fully grown SPs (self-termination stage, stage f). For each stage, geometrical assumptions and physical specifications are described in the Supplementary Information. The van der Waals (VdW) interaction energies between two dissimilar spheres are evaluated with the following equation.[67]

$$V vdw = -\frac{A_{132}}{6x} \frac{(R_1 R_2)}{(R_1 + R_2)} \tag{1}$$

where A_{132} is the Hamaker's constant of material 1 and 2 across medium 3, R_i is the radius and x is the closest distance between the two spheres. Here, 1, 2 and 3 are Au, Fe_3O_4, and water respectively. The double layer electrical energies between two dissimilar spheres is represented from the following equation.[68]

$$V_{DL} = \frac{\pi \varepsilon_0 \varepsilon_r R_1 R_2}{(R_1 + R_2)} (\zeta_1^2 + \zeta_2^2)$$
$$\times \left\{ \frac{2\zeta_1 \zeta_2}{\zeta_1^2 + \zeta_2^2} ln \left(\frac{1 + e^{-\kappa x}}{1 - e^{-\kappa x}} \right) + ln \left(1 - e^{-2\kappa x} \right) \right\} \tag{2}$$

where ε_0 is the permittivity of vacuum, ε_r is the dielectric constant of water, ζ_i is the zeta potential. Practical Debye Length, $\kappa^{-1} \approx 100$ nm,[69] is used to account for dissolved CO_2 that converts to carbonic acid. The total interaction potential is given by

$$V_{DLVO} = V_{vdw} + V_{DL} \tag{3}$$

The analysis shows that the interaction at stage i has the most attractive potential, **Figure 2**a, and energetically accounts for mechanism that initiates the self-assembly. Also note that the

direct assembly of Au NPs produced by the hydroquinone reaction of the surface of bare Fe_3O_4 NPs failed. The Au is known to have one of the highest Hamaker's constant and its smooth shell on Fe_3O_4 was necessary to strengthen the VdW interaction energies and overcome the electrostatic repulsion because of the similarity of charges on the citrate-stabilized NPs and newly formed Au NPs reduced by hydroquinone. Figure 2b shows that the attractive potential is indeed superior with the presence of Au shell.

The formation of spiky SPs by attaching free NPs made extraneously in solution is confirmed by presence of facets, seen in the HR-TEM images in **Figure 3**. The individual constituent NPs retained in the assembled structure were monocrystalline. A filtered lattice image (Figure 3b, take from the square in Figure 3a) revealed that fringes are caused by the reciprocal lattice points only (branch of the spiky SPs). Its fast Fourier transform (FTT) pattern is shown in the inset of Figure 3b. This high-resolution image of Au spikes clearly shows the uniform lattice structure of a single crystal. The fringe spacing was measured to be 0.196 nm, which corresponds to the spacing between the (200) planes of the face-centered cubic Au (0.204 nm) (JCPDS card no. 04–0784). At the same time, the selected area electron diffraction (SAED) pattern of all the spiky SPs revealed polycrystallinity, as evidenced by the gradual epitaxial atom-by-atom growth of the Au spikes on the previously formed smooth Fe_3O_4@Au NPs (Figure 3c). The SAED pattern is superposition of Au and Fe_3O_4 lattices, showing five distinguishable planes of (111), (200), (220), (311), (222) from Au and one distinguishable (311) plane from Fe_3O_4. Other planes overlap with the Au planes.[71]

The XRD diffraction data also confirmed that the spiky SPs were polycrystalline. The XRD peaks from the SPs fitted well to those of the Au and Fe_3O_4 bulk phases (Figure 3d). The Au diffraction peaks matched the reflections of the (111), (200), (220), (311), and (222) planes. The Fe_3O_4 diffraction peaks can be ascribed to the (220), (311), and (440) planes.[72,73] The
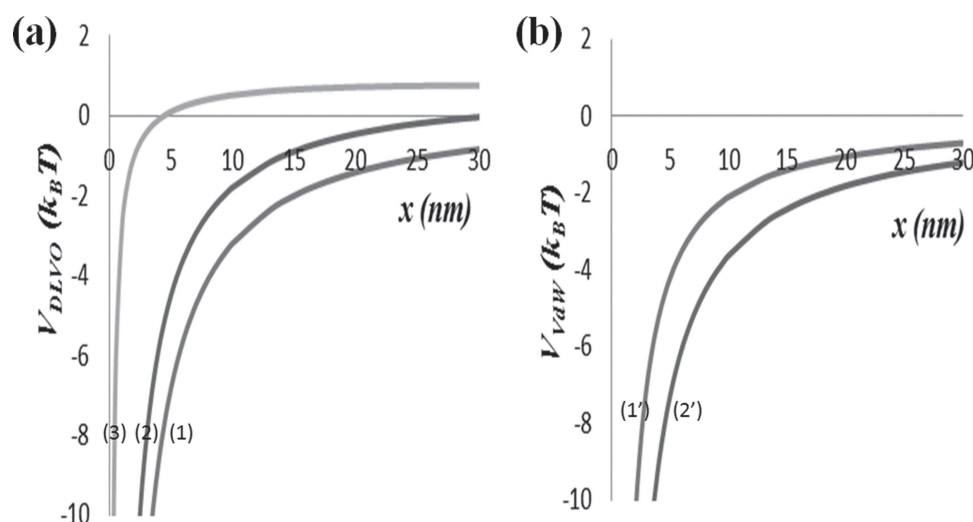
Figure 2. a) V_{DLVO} through the progressive stages; *stage i* (line (1)), *stage g* (line (2)), *stage f* (line (3)). The initial core-shell stage has the most attractive potential. The self-termination stage is explained via the repulsive potential between the SPs and the hydroquinone reduced Au NPs. b) V_{vdW} at *stage 0* (line (1')) and *stage i* (line(2')). The *stage 0* represents the interaction between bare Fe_3O_4 NPs and hydroquinone reduced Au NPs. The VdW attraction is enhanced with the presence of Au shell around the Fe_3O_4 NP.

www.MaterialsViews.com

ADVANCED
FUNCTIONAL
MATERIALS
www.afm-journal.de

FULL PAPER
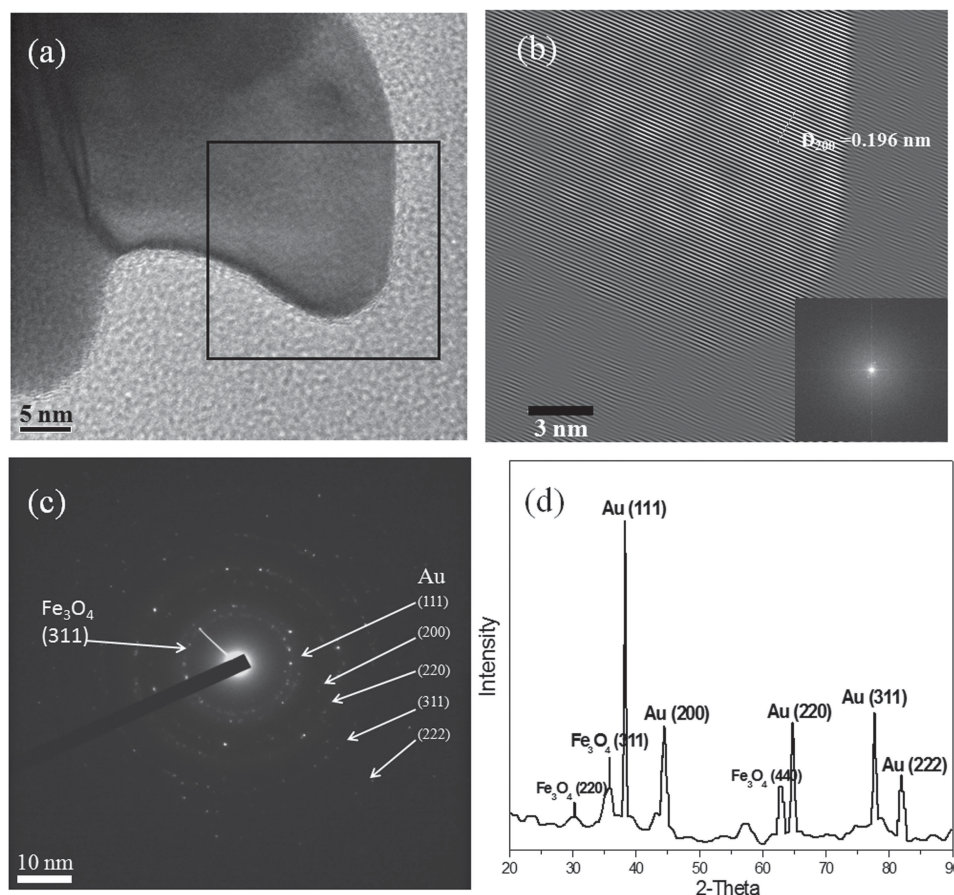
Figure 3. a) HR-TEM image of one branch of spiky SPs; b) filtered lattice image reveals fringes due only to the reciprocal lattice points of black square in (a) and the FFT pattern of selected area within (a); c) selected area electron diffraction (SAED) pattern of spiky SPs; and d) XRD pattern of spiky SPs.

assembly route for the formation of the spiky SPs was further substantiated by the negative control experiment: spiky SPs were absent in the reaction media when no strong reducing agent–hydroquinone–was present; however, the reduction of $HAuCl_4$ was still initiated in the presence of smooth Fe_3O_4@ Au core–shell particles. There, when atom-by-atom growth mode on the existing Au shell was possible but individual constituent NPs in solution were absent (Figure S5, Supporting Information),[58] the spiky morphology does not appear. For the additional confirmation of the self-assembly mechanism, we observe the gradual time-dependent size increase of the spiky SP growth by TEM (Figure S6, Supporting Information), indicating that the length of the spikes (ca. 10 nm) was approximately the same at the initial and final stages of SP formation, which corresponds very well to the size of individual Au NPs generated in solution.

2.3. Deviations from the Expected Self-Assembly Mechanism and its Synthetic Implications

We anticipated that the agglomeration/assembly of the in situ-generated Au NPs on Fe_3O_4@Au core–shell particles would have the same self-limiting kinetics previously observed.[37,38,74]

In other words, the size of the SPs would reach a critical point when the electrostatic repulsion between the SPs and the free NPs in solution would be the dominating force. This is attributed to decrease in the effective Hamaker's constant leading to reduction in the VdW interaction energies between the SPs and hydroquinone reduced Au NPs (Figure 2a). However, their formation mechanism did not confirm these expectations, and we found important differences with the previously observed assembly process. We did not see any evidence of gaps between the newly attached Au NPs or between them and the original smooth Fe_3O_4@Au core. However, these gaps were clearly visible in the previous examples of SPs made from semiconductor NPs, as well as in SPs made from the combination of a semiconductor and Au NPs.[39] We attribute this difference to (a) the dynamic nature of citrate as a stabilizing agent and (b) the presence of high-energy crystalline facets in the newly formed NPs. As such, the crystalline facet corresponding to the high-energy (200) plane accounted for the strong signal in the HRTEM and electron diffractogram. The current results represent a new case in which SPs transform after assembling into a continuous structural unit. The integration of the lattices (although not necessarily epitaxial) of the pre-made cores with smooth Au shells and newly attached, fairly large NPs could be compared to the analogous process observed in the assembly of PbS NPs.[37]
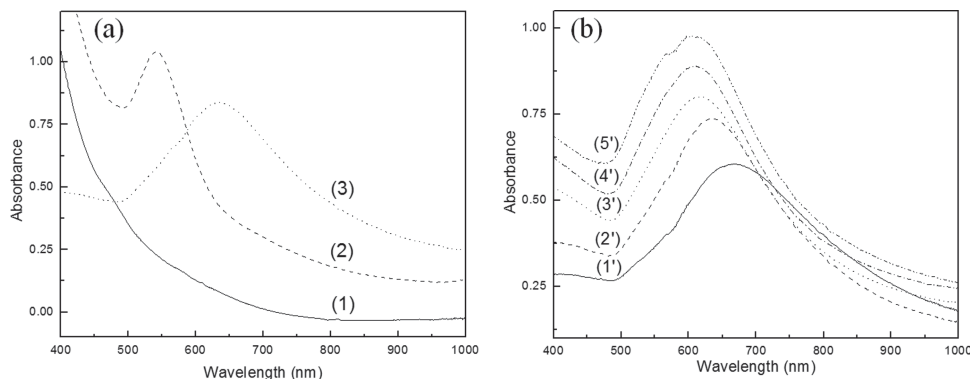
ADVANCED
FUNCTIONAL
MATERIALS
www.afm-journal.de

Materials
Views
www.MaterialsViews.com
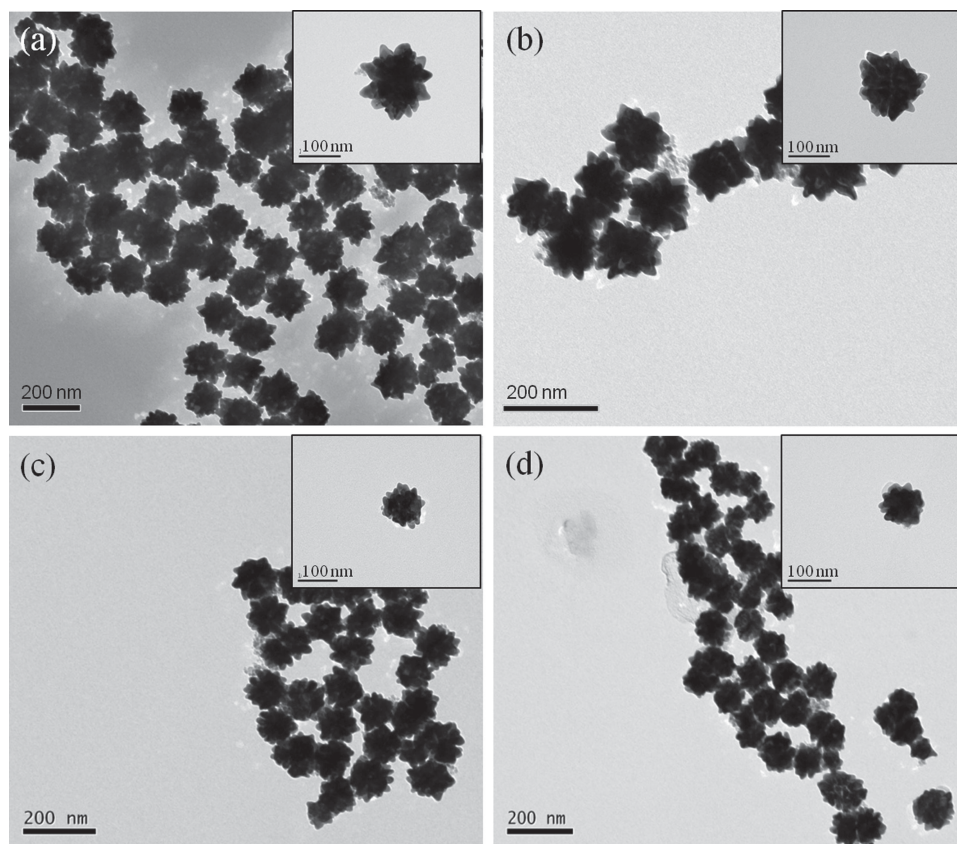
Figure 4. TEM images of spiky SPs assembled in the presence of different amounts of smooth Fe_3O_4@Au core–shell particles: (a) 4.5 nM, (b) 8.9 nM, (c) 13.2 nM, and (d) 17.5 nM. Insets show magnified images of corresponding individual SPs. [Volume of smooth Fe_3O_4@Au seeds increased from 100 to 400 μL in 100 μL increments for spectra (a)–(d).]

The transformation from the SP with gaps to the assembly without gaps let us to rethink the strategy for the control of the SP diameters. Although it could be beneficial for their optical and/or electrical properties, lattice-to-lattice connectivity between the NPs forming the SPs diminishes their ability to dis-assemble as their overall charge increases, which, therefore, eliminates the local thermodynamic minimum corresponding to the equal energy of attachment of NPs and detachment of previously assembled NPs. However, it leaves the possibility of controlling the SP diameter by limiting the pool of additional Au NPs available for assembly. For instance, it could be done by varying the ratio of smooth Fe_3O_4@Au NPs to the total number of new Au NP being reduced by hydroquinone. Indeed, as the amount of smooth Fe_3O_4@Au seeds increased from 100 to 500 μL while keeping the quantities of $HAuCl_4$ and hydroquinone fixed, we were able to decrease the average diameter of the spiky SPs from 175 ± 9.1 nm to 95 ± 6.3 nm (**Figure 4**). Correspondingly, the color of the solution shifted from green to blue and the maximum wavelength of absorption in the UV-visible absorption spectra changed from 670 to 600 nm (**Figure 5**b). Having fewer Au NPs available for attachment to the Au surface, led to the growth of each SP to large diameters, which is similar to the growth mechanism of individual NPs,[58,70] and thus had to follow the same growth equations.[37] A qualitatively

similar effect could be obtained by using different concentrations of hydroquinone. The concentration of the reducing agent limited the number of constituent Au NPs formed, and, therefore, limited the size of the resulting SPs while maintaining the uniformity of their diameters and overall morphology (**Figure 6**). As the amount of the 30 mM hydroquinone solution increased from 125 to 1000 μL, the diameter of the SPs increased from 105 ± 5.9 nm to 185 ± 11.4 nm. The length and the number of spikes (Figures 6b,c,d) increased as the plasmon absorption of the NPs shifted from 605 to 650 nm (Figure 6a).

2.4. Magnetoplasmonic Properties

The synthesis of spiky shapes of magneto-plasmonic particles is particularly attractive for obtaining large optical cross sections for NIR photons necessary for applications in biomedical imaging and drug delivery[40,41] because of the transparency of biological tissues at these wavelengths.[42] Concomitantly, Fe_3O_4 NPs are useful as T_2-weighted contrast agents in magnetic resonance imaging, magnetofection, and cell sorting[43,44] including detection of rare cells, owing to their unique magnetic properties and biocompatibility. Combining these magnetic properties with spiky plasmonic shells of Au will enable better cancer

Materials
Views
www.MaterialsViews.com

ADVANCED
FUNCTIONAL
MATERIALS
www.afm-journal.de

FULL PAPER

Figure 5. a) UV-visible spectra of (1) aqueous dispersions with Fe_3O_4 NPs, (2) nearly spherical smooth $Fe_3O_4@Au$ core–shell particles, and (3) spiky SPs. b) UV-visible absorption spectra of spiky SPs solutions assembled in the presence of different amounts of smooth $Fe_3O_4@Au$ core–shell particles serving as seeds for the assembly of SPs: (1') 4.5 nM; (2') 8.9 nM; (3') 13.2 nM; (4') 17.5 nM; and (5') 21.7 nM. [Volume of smooth $Fe_3O_4@Au$ seeds increased from 100 to 500 μL in 100 μL increments for spectra (1′) to (5′).]

diagnosis/therapy,[45] imaging,[46,47] DNA analysis,[48,49] and drug delivery.[50,51] In addition, the dielectric properties and chemical stability of nanostructures made of spiky Fe_3O_4–Au SPs makes them ideal substrates for the study of well-defined plasmon resonances within the visible and NIR spectral ranges with high electromagnetic fields in the vicinity of NP apexes. The spiky Fe_3O_4–Au nanostructures can be used for surface-enhanced Raman scattering (SERS),[52,53] heterogeneous catalysts, and DNA colorimetric sensing devices.[41,54] A strong SERS activity can be detected with intensity over 10^7 and a relatively high reproducibility.[55,56] In addition, the spiky-like structure leads to large SPR shift from 500 to 800 nm and tunable SPR enhancement light scattering and absorption, making them novel and high effective contrast agents for in vivo cancer diagnosis and therapy. Moreover, the spiky metallic nanoparticles, with increased surface area-to volume ratio, a larger number of surface defects, and tips with selected crystallinity, display excellent catalytic properties compare with spherical particles.[57]

The optical response of the spiky SPs is dominated by the plasmon mode associated with the gold tips and can be rationalized in terms of plasmon hybridization: a concept originally developed for nanoshells.[75,76] The plasmons of spiky SPs arise due to the hybridization of the plasmons supported by the inner radius (gold cavity), the outer radius of the shell layer (spiky gold surface) and lower frequency plasmon oscillations at the tips. This hybridization results in a complex, multipeaked optical spectrum where the thickness of the intermetallic dielectric layer controls the mode coupling, and the tip aperture angle and length effects can induce red-shifting of the collective plasmon modes. The tips are also responsible for an increase in the extinction cross section (a fourfold increase with respect to the individual tip plasmons).

Thus, the spiky SPs showed that the plasmon bands were red-shifted with respect to those for spheres $Fe_3O_4@Au$ core–shell particles. They also showed very high electromagnetic fields localized at each tip. From the UV-visible absorption spectra of spiky SPs (Figures 5 and 6a), we can clearly see that spiky SPs display three distinct plasmonic features: an intense band typically centered around 600–670 nm and two weaker shoulders located at ca. 566 and 800 nm. It might is expected that the tip aperture angle and length strongly were found to

strongly affect the energy of the plasmon hybridization mode at the tip, whereas the core size has a milder influence and the number of tips modulates the intensity of plasmonic tip modes.

The measurement of the magnetic properties of the spherical $Fe_3O_4@Au$ NPs and spiky $Fe_3O_4@Au$ SPs using the SQUID technique allowed us to assess the saturation magnetization, coercivity, susceptibility, and blocking temperature of the NPs. **Figure 7**a shows the spherical $Fe_3O_4@Au$ NPs and spiky $Fe_3O_4@Au$ SPs hysteresis loops measured at room temperature. The saturation magnetization (Ms) of spherical $Fe_3O_4@Au$ NPs was 16.2 emu g^{-1} at room temperature. Like the spherical $Fe_3O_4@Au$ NPs, spiky $Fe_3O_4@Au$ SPs were nearly paramagnetic at room temperature, and had an Ms of 5.2 emu g^{-1}. This suggests that the Ms of spherical $Fe_3O_4@Au$ NPs drops slightly when the surface is coated with Au. It also indicates that exchange interactions with the ligand or outer layers, like the gold coating, at the surface did not affect the movement of the inner Fe_3O_4 NPs too much.[77] Moreover, the spherical $Fe_3O_4@Au$ NPs and spiky $Fe_3O_4@Au$ SPs that were separated using a magnet are shown in inset (1) and (2) of Figure 7b. These results show that the $Fe_3O_4@Au$ NPs were separable using high-gradient magnetic filtration. After magnetic separation, the $Fe_3O_4@Au$ NPs were still well dispersed in aqueous solutions. The spiky $Fe_3O_4@Au$ SPs had a surface plasmon peak at the high wavelength of 640 nm a sharp band compared to the separated spiky $Fe_3O_4@Au$ SPs solution (Figure 7b).

3. Conclusions

We have demonstrated a new method for the formation of spiky nanoscale particles, which represent some of the interesting non-Platonic, non-Archimedean, non-spherical, concave shapes. The formation of these particles was accomplished using a SP self-assembly approach, in which additional negatively charged Au NPs were attached to the surface of previously fabricated, negatively charged smooth $Fe_3O_4@Au$ core–shell particles. The mechanism reveals essential differences with the interpretation of the origin of spiky or bristled morphology of nanoscale structures and is likely to be applicable to other types of nanoscale structures. It is also generic and can be applied
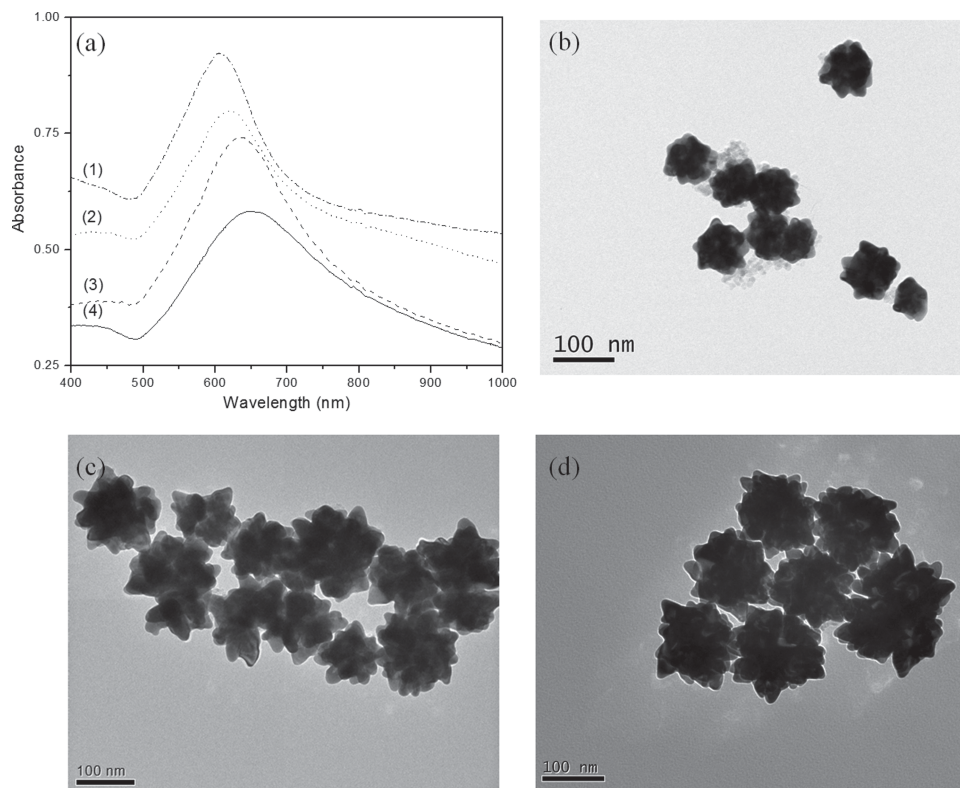
Figure 6. a) UV-visible absorption spectra of spiky SPs assembled for different amounts of hydroquinone: (1) 0.37 mM, (2) 0.72 mM, (3) 1.41 mM, and (4) 2.7 mM. The amount of seeds and sodium citrate stabilizer were fixed at 100 and 22 µL, respectively. b–d) TEM images of spiky SPs prepared with different volumes of hydroquinone: (b) 0.37 mM, (c) 1.41 mM, and (d) 2.7 mM. [The volume of hydroquinone: (1) 125 µL; (2) 250 µL; (3) 500 µL; and (4) 1000 µL.]

for the preparation of nano- and submicrometer particles with multiple functionalities and complex geometries.

Understanding of the SP self-assembly route makes the process of their preparation simple, fast, and easily controllable rather than empirical and fortuitous. It also makes possible to avoid utilization of polymeric compounds[78,79] such as PVP that was considered to be essential before[5] as well as non-aqueous solvents[80–82] that are less desirable than aqueous dispersion of nanoscale assemblies with short easily replaceable stabilizers, especially for biological applications considering the presence of the Fe_3O_4 superparamagnetic core.

Unlike the previous cases of SP formation, we observed here a non-epitaxial merger of the Au lattices upon assembly. This process was attributed to the weak stabilization of the newly formed NPs and the presence of high-energy (200) facets. Although it is beneficial for potential applications, the lattice-to-lattice connectivity of the constituent NPs limited their ability to disassemble, making thermodynamic control of their diameters difficult. To avoid this limitation, we reduced the number of constituent NPs available for assembly on the pre-made cores and demonstrated variation of diameters between 95 and 185 nm while maintaining the uniformity of their morphology
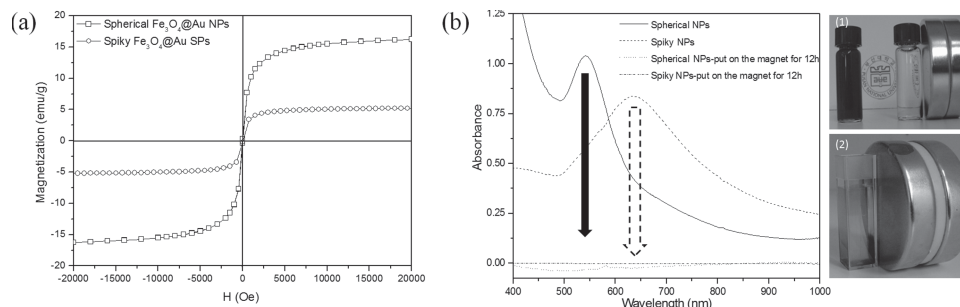
Figure 7. a) Measured magnetization moments of spherical Fe_3O_4@Au core–shell NPs and spiky Fe_3O_4@Au SPs as a function of applied magnetic field at room temperature. b) UV-vis spectrum of an aqueous dispersion from Fe_3O_4@Au core–shell particles after being subjected to a magnetic field for 12 h. Images on the right depict the dispersions of (1) spherical Fe_3O_4@Au core–shell particles and (2) spiky SPs in magnetic field.

Materials
Views

www.MaterialsViews.com

ADVANCED
FUNCTIONAL
MATERIALS

www.afm-journal.de

and diameters. The reported spiky SPs can be used in multiple applications including SERS biosensing, catalysis, magnetic separation, and targeted drug delivery.

4. Experimental Section

Materials: Hydrogen tetrachloroaurate(III) trihydrate (HAuCl$_4$·3H$_2$O, 99.9%), sodium citrate (Na$_3$C$_6$H$_5$O$_7$), FeCl$_3$·6H$_2$O, and hydroquinone (98%) were supplied by Sigma-Aldrich (South Korea). FeCl$_2$·4H$_2$O was purchased from Wako Pure Chemical Industries, Ltd. (Japan). A 28% w/v% ammonia solution was purchased from Duksan Pure Chemical Co., Ltd. (South Korea). Deionized water (>18.2 mΩ/cm) was used throughout the experimental procedure. All the chemicals were of analytical grade and used as received.

Synthesis of Fe$_3$O$_4$ Nanoparticles: Fe$_3$O$_4$ magnetic NPs were synthesized using the co-precipitation method.[53] In a typical synthesis, 1.622 g of FeCl$_3$·6H$_2$O and 0.994 g of FeCl$_2$·4H$_2$O were dissolved in 40 mL of water under constant mechanical stirring. Then, 5 mL of the ammonia solution (28% w/v%) was quickly added to the reaction mixture, and the resulting solution was left undisturbed for 10 min. Sodium citrate (4.4 g) was subsequently added to the reaction mixture. The reaction temperature was then raised to 90 °C, and the solution was allowed to react for 30 min under continuous stirring. The resulting black precipitate, obtained by cooling the reaction mixture to room temperature, was thoroughly rinsed with copious amounts of water several times. The precipitate was separated from the supernatant after each rinsing step using a permanent magnet. Finally, the black-colored precipitate was dried under vacuum at room temperature.

Preparation of Fe$_3$O$_4$@Au Core–Shell Particles: Deposition of a smooth layer of gold on the Fe$_3$O$_4$ NPs was performed via reduction of Au^{3+} on their surface by using a modification of a previously described procedure.[72] Briefly, a 20 mL aliquot of a 0.5 mM HAuCl$_4$ solution was heated until it boiled and 10 mL of 0.136 µM of the Fe$_3$O$_4$ solution was rapidly added to it under vigorous stirring. The reaction mixture gradually changed from brown to burgundy. After 10 min when the color of the solution stopped changing, the heater was removed while continuing the stirring action for an additional 10 min as the solution cooled down to room temperature. The Fe$_3$O$_4$@Au NPs were separated using a magnet. They were subsequently re-dispersed and centrifuged thrice at 6500 rpm (108 s^{-1}) for 20 min. The resulting precipitate was washed and re-suspended in deionized water. The final NP dispersion was dark purple color.

Preparation of Spiky Fe$_3$O$_4$@Au Supraparticles: Preparation of spiky SPs was performed via reduction of Au^{3+} in the presence of smooth spherical Fe$_3$O$_4$@Au core–shell particles serving as seeds similar to the approach reported previously.[83,84] First, a 30 mM aqueous hydroquinone solution was prepared by dissolving 33 mg of solid hydroquinone in 10 mL of deionized water. This solution must be used within 1 day. For a typical synthesis of spiky SPs, 10 mL of aqueous HAuCl$_4$ (0.25 mM) was stirred vigorously and 100–500 µL of Fe$_3$O$_4$@Au seeds (the smooth, spherical core–shell particles), 22 µL of 1% sodium citrate solution, and 1 mL of the previously prepared 30 mM hydroquinone solution were added sequentially. The resulting solution was stirred at room temperature for 30 min. The diameter and surface roughness of Fe$_3$O$_4$@Au NPs were tuned by altering the seeds/hydroquinone ratio, which changes the total number of Au NPs produced in the reaction system.

Optical and Microscopic Characterization: Absorbance of the Fe$_3$O$_4$@Au SPs was measured by UV-vis spectroscopy (S310, SCINCO, Korea). The morphologies and sizes of the NPs were characterized using HR-TEM (JEM-3010, JEOL, Japan) and AFM (diInnova, Veeco). The surface potentials and particle size distribution of the NPs were monitored by a zeta-sizer (Nano ZS, Malvern Instruments, Great Britain). An X-ray powder diffractometer with Cu Ka radiation and a Ni filter (D8 FOCUS 2.2 kW, Bruker, Germany) were used to characterize the Fe$_3$O$_4$@Au SPs. The data were collected at 2θ from 10° to 90° at a scan rate of 0.06° per step and 2 s per point. Magnetic measurements were performed using a superconducting quantum interference device (SQUID) magnetometer (MPMS XL-7, Quantum Design, USA).[85]

Supporting Information

Supporting Information is available from the Wiley Online Library or from the author.

[1] J. de Graaf, R. van Roij, M. Dijkstra, *Phys. Rev. Lett.* **2011**, *107*, 155501.

[2] P. F. Damasceno, M. Engel, S. C. Glotzer, *Science* **2012**, *337*, 453.

[3] U. Agarwal, F. A. Escobedo, *Nat. Mater.* **2011**, *10*, 230.

[4] Q. Wei, H. M. Song, A. P. Leonov, J. A. Hale, D. Oh, Q. K. Ong, K. Ritchie, A. Wei, *J. Am. Chem. Soc.* **2009**, *131*, 9728.

[5] N. Pazos-Pérez, S. Barbosa, L. Rodriguez-Lorenzo, P. Aldeanueva-Potel, J. Pérez-Juste, I. Pastoriza-Santos, R. A. Alvarez-Puebla, L. M. Liz-Marzán, *J. Phys. Chem. Lett.* **2010**, *1*, 24.

[6] P. S. Kumar, I. Pastoriza-Santos, B. Rodriguez-González, F. J. G. de Abajo, L. Liz-Marzán, *Nanotechnology* **2007**, *19*, 015606.

[7] C. L. Nehl, H. Liao, J. H. Hafner, *Nano Lett.* **2006**, *6*, 683.

[8] H. Zhao, S. Yang, H. You, Y. Wu, B. Ding, *Green Chem.* **2012**, *14*, 3197.

[9] H. M. Song, Q. Wei, Q. K. Ong, A. Wei, *ACS Nano* **2010**, *4*, 5163.

[10] S. E. Habas, H. Lee, V. Radmilovic, G. A. Somorjai, P. Yang, *Nat. Mater.* **2007**, *6*, 692.

[11] M. J. Mulvihill, X. Y. Ling, J. Henzie, P. Yang, *J. Am. Chem. Soc.* **2009**, *132*, 268.

[12] J. Lee, H. Zhou, J. Lee, *J. Mater. Chem.* **2011**, *21*, 16935.

[13] Y. Xia, Y. Xiong, B. Lim, S. E. Skrabalak, *Angew. Chem. Int. Ed.* **2009**, *48*, 60.

[14] C. Burda, X. Chen, R. Narayanan, M. A. El-Sayed, *Chem. Rev.* **2005**, *105*, 1025.

[15] A. R. Tao, S. Habas, P. Yang, *Small* **2008**, *4*, 310.

[16] J. Lee, N. A. Kotov, *Nano Today* **2007**, *2*, 48.

[17] N. Tian, Z. Y. Zhou, N. F. Yu, L. Y. Wang, S. G. Sun, *J. Am. Chem. Soc.* **2010**, *132*, 7580.

FULL PAPER

[18] T. Ming, W. Feng, Q. Tang, F. Wang, L. Sun, J. Wang, C. Yan, *J. Am. Chem. Soc.* **2009**, *131*, 16350.

[19] Z. Y. Zhou, Z. Z. Huang, D. J. Chen, Q. Wang, N. Tian, S. G. Sun, *Angew. Chem.* **2010**, *122*, 421.

[20] Y. Ma, Q. Kuang, Z. Jiang, Z. Xie, R. Huang, L. Zheng, *Angew. Chem. Int. Ed.* **2008**, *47*, 8901.

[21] D. Y. Kim, S. H. Im, O. O. Park, *Cryst. Growth. Des.* **2010**, *10*, 3321.

[22] J. Zhang, M. R. Langille, M. L. Personick, K. Zhang, S. Li, C. A. Mirkin, *J. Am. Chem. Soc.* **2010**, *132*, 14012.

[23] C. L. Lu, K. S. Prasad, H. L. Wu, J. A. A. Ho, M. H. Huang, *J. Am. Chem. Soc.* **2010**, *132*, 14546.

[24] Y. Yu, Q. Zhang, B. Liu, J. Y. Lee, *J. Am. Chem. Soc.* **2010**, *132*, 18258.

[25] F. Wang, C. Li, L. D. Sun, H. Wu, T. Ming, J. Wang, J. C. Yu, C. H. Yan, *J. Am. Chem. Soc.* **2010**, *133*, 1106.

[26] H. Y. Wu, M. Liu, M. H. Huang, *J. Phys. Chem. B* **2006**, *110*, 19291.

[27] S. Srivastava, A. Santos, K. Critchley, K. S. Kim, P. Podsiadlo, K. Sun, J. Lee, C. Xu, G. D. Lilly, S. C. Glotzer, N. A. Kotov, *Science* **2010**, *327*, 1355.

[28] N. A. Kotov, *Science* **2010**, *330*, 188.

[29] N. Tian, Z. Y. Zhou, S. G. Sun, *J. Phys. Chem. C* **2008**, *112*, 19801.

[30] N. Tian, Z. Y. Zhou, S. G. Sun, L. Cui, B. Ren, Z. Q. Tian, *Chem. Commun.* **2006**, 4090.

[31] Y. Wang, Z. Tang, X. Liang, L. M. Liz-Marzan, N. A. Kotov, *Nano Lett.* **2004**, *4*, 225.

[32] P. Aldeanueva-Potel, E. Carbó-Argibay, N. Pazos-Pérez, S. Barbosa, I. Pastoriza-Santos, R. Varez-Puebla, L. Liz-Marzán, *ChemPhysChem* **2012**, *13*, 2561.

[33] H. M. Chen, R. S. Liu, D. P. Tsai, *Cryst. Growth. Des.* **2009**, *9*, 2079.

[34] W. Du, X. Qian, X. Niu, Q. Gong, *Cryst. Growth. Des.* **2007**, *7*, 2733.

[35] N. G. Bastús, J. Comenge, V. Puntes, *Langmuir* **2011**, *27*, 11098.

[36] A. Guerrero-Martínez, S. Barbosa, I. Pastoriza-Santos, L. M. Liz-Marzán, *Curr. Opin. Colloid Interface Sci.* **2011**, *16*, 118.

[37] A. Querejeta-Fernández, J. C. Hernández-Garrido, H. Yang, Y. Zhou, A. Varela, M. Parras, J. Calvino-Gámez, J. M. González-Calbet, P. F. Green, N. A. Kotov, *ACS Nano* **2012**, *6*, 3800.

[38] Z. Tang, Z. Zhang, Y. Wang, S. C. Glotzer, N. A. Kotov, *Science* **2006**, *314*, 274.

[39] Y. Xia, T. D. Nguyen, M. Yang, B. Lee, A. Santos, P. Podsiadlo, Z. Tang, S. C. Glotzer, N. A. Kotov, *Nat. Nanotechnol.* **2011**, *6*, 580.

[40] E. C. Dreaden, A. M. Alkilany, X. Huang, C. J. Murphy, M. A. El-Sayed, *Chem. Soc. Rev.* **2012**, *41*, 2740.

[41] W. Chen, N. Xu, L. Xu, L. Wang, Z. Li, W. Ma, Y. Zhu, C. Xu, N. A. Kotov, *Macromol. Rapid Commun.* **2010**, *31*, 228.

[42] J. H. Jung, J. H. Lee, S. Shinkai, *Chem. Soc. Rev.* **2011**, *40*, 4464.

[43] D. Yoo, J. H. Lee, T. H. Shin, J. Cheon, *Acc. Chem. Res.* **2011**, *44*, 863.

[44] C. Tassa, S. Y. Shaw, R. Weissleder, *Acc. Chem. Res.* **2011**, *44*, 842.

[45] B. Godin, E. Tasciotti, X. Liu, R. E. Serda, M. Ferrari, *Acc. Chem. Res.* **2011**, *44*, 979.

[46] G. K. Kouassi, J. Irudayaraj, *Anal. Chem.* **2006**, *78*, 3234.

[47] I. Robinson, L. D. Tung, S. Maenosono, C. Wälti, N. T. K. Thanh, *Nanoscale* **2010**, *2*, 2624.

[48] M. Riepl, M. Östblom, I. Lundström, S. C. T. Svensson, A. W. D. van der Gon, M. Schäferling, B. Liedberg, *Langmuir* **2005**, *21*, 1042.

[49] L. C. Cheng, J. H. Huang, H. M. Chen, T. C. Lai, K. Y. Yang, R. S. Liu, M. Hsiao, C. H. Chen, L. J. Her, D. P. Tsai, *J. Mater. Chem.* **2012**, *22*, 2244.

[50] K. C.-F. Leung, S. Xuan, X. Zhu, D. Wang, C. P. Chak, S. F. Lee, W. K. W. Ho, B. C. T. Chung, *Chem. Soc. Rev.* **2012**, *41*, 1911.

[51] G. Maiorano, L. Rizzello, M. A. Malvindi, S. S. Shankar, L. Martiradonna, A. Falqui, R. Cingolani, P. P. Pompa, *Nanoscale* **2011**, *3*, 2227.

[52] J. J. Storhoff, R. Elghanian, R. C. Mucic, C. A. Mirkin, R. L. Letsinger, *J. Am. Chem. Soc.* **1998**, *120*, 1959.

[53] H. Zhou, J. Lee, T. J. Park, S. J. Lee, J. Y. Park, J. Lee, *Sens. Actuators B—Chem.* **2012**, *163*, 224.

[54] A. Agarwal, X. Shao, J. R. Rajian, H. Zhang, D. L. Chamberland, N. A. Kotov, X. Wang, *J. Biomed. Opt.* **2011**, *16*, 051307.

[55] E. Nalbant Esenturk, A. R. Hight Walker, *J. Raman Spectrosc.* **2009**, *40*, 86.

[56] L. Brus, *Acc. Chem. Res.* **2008**, *41*, 1742.

[57] R. Narayanan, M. A. El-Sayed, *J. Phys. Chem. B* **2005**, *109*, 12663.

[58] S. D. Perrault, W. C. W. Chan, *J. Am. Chem. Soc.* **2009**, *131*, 17042.

[59] C. S. Levin, C. Hofmann, T. A. Ali, A. T. Kelly, E. Morosan, P. Nordlander, K. H. Whitmire, N. J. Halas, *ACS Nano* **2009**, *3*, 1379.

[60] P. Sharma, V. Bhalla, V. David, G. Shekhawat, E. S. Prasad, C. R. Suri, *Sci. Rep.* **2012**, *2*, 877.

[61] J. Gallo, I. García, D. Padro, B. Arnáiz, S. Penadés, *J. Mater. Chem.* **2010**, *20*, 10010.

[62] S. T. Gentry, S. J. Fredericks, R. Krchnavek, *Langmuir* **2009**, *25*, 2613.

[63] A. J. Bard, H. Zhou, S. J. Kwon, *Isr. J. Chem.* **2010**, *50*, 267.

[64] X. Xiao, A. J. Bard, *J. Am. Chem. Soc.* **2007**, *129*, 9610.

[65] E. Gachard, H. Remita, J. Khatouri, B. Keita, L. Nadjo, J. Belloni, *New J. Chem.* **1998**, *22*, 1257.

[66] A. Mechler, A. A. Torriero, A. Nafady, C. Y. Lee, A. M. Bond, A. P. O' Mullane, S. Bhargava, *Colloid Surf. A—Physicochem.Eng. Asp.* **2010**, *370*, 35.

[67] J. N. Israelachvili, *Intermolecular and Surface Forces: Revised*, 3rd edition, Academic Press, San Diego **2011**,

[68] J. Goodwin, *Colloids and Interfaces with Surfactants and Polymers*, Wiley, West Sussex **2009**.

[69] H. C. Chang, G. Yossifon, E. A. Demekhin, *Annu. Rev. Fluid Mech.* **2012**, *44*, 401.

[70] G. Frens, *Nat. Phys. Sci.* **1973**, *241*, 20

[71] C. Huang, J. Jiang, C. Muangphat, X. Sun, Y. Hao, *Nanoscale Res Lett* **2011**, *6*, 1.

[72] J. Li, J. Wu, X. Zhang, Y. Liu, D. Zhou, H. Sun, H. Zhang, B. Yang, *J. Phys. Chem. C* **2011**, *115*, 3630.

[73] K. R. Brown, D. G. Walter, M. J. Natan, *Chem. Mater.* **2000**, *12*, 306.

[74] Z. Tang, N. A. Kotov, M. Giersig, *Science* **2002**, *297*, 237.

[75] E. Prodan, C. Radloff, N. J. Halas, P. Nordlander, *Science* **2003**, *302*, 419.

[76] N. J. Halas, S. Lal, S. Link, W. S. Chang, D. Natelson, J. H. Hafner, P. Nordlander, *Adv. Mater.* **2012**, *24*, 4842.

[77] W. C. Huang, P. J. Tsai, Y. C. Chen, *Small* **2009**, *5*, 51.

[78] J. Shan, H. Tenhu, *Chem. Commun.* **2007**, *0*, 4580.

[79] S. Xing, L. H. Tan, M. Yang, M. Pan, Y. Lv, Q. Tang, Y. Yang, H. Chen, *J. Mater. Chem.* **2009**, *19*, 3286.

[80] V. Mazumder, M. Chi, K. L. More, S. Sun, *Angew. Chem.* **2010**, *122*, 9558.

[81] Y. Jin, C. Jia, S. W. Huang, M. O'Donnell, X. Gao, *Nat. Commun.* **2010**, *1*, 41.

[82] R. Hao, R. Xing, Z. Xu, Y. Hou, S. Gao, S. Sun, *Adv. Mater.* **2010**, *22*, 2729.

[83] K. C. Grabar, R. G. Freeman, M. B. Hommer, M. J. Natan, *Anal. Chem.* **1995**, *67*, 735.

[84] H. Zhou, J. Dong, V. K. Deo, E. Y. Park, J. Lee, *Sens. Actuators B—Chem.* **2012**, *178*, 192.

[85] W. Lianyan, J. Luo, Q. Fan, M. Suzuki, I. S. Suzuki, M. H. Engelhard, Y. Lin, N. Kim, J. Q. Wang, C. J. Zhong, *J. Phys. Chem. B* **2005**, *109*, 21593.